Journal of Sol-Gel Science and Technology 33, 283–298, 2005

Gel Structure, Gel Decomposition and Phase Formation Mechanisms in the Aqueous Solution–Gel Route to Lanthanum Substituted Bismuth Titanate

A. HARDY, G. VANHOYLAND, E. GEUZENS, M.K. VAN BAEL, J. MULLENS* AND L.C. VAN POUCKE
Laboratory of Inorganic and Physical Chemistry, IMO Limburgs Universitair Centrum, B-3590 Diepenbeek, Belgium
jules.mullens@luc.ac.be

J. D'HAEN
IMEC, Division IMOMEC, Limburgs Universitair Centrum, B-3590 Diepenbeek, Belgium

Received October 6, 2003; Accepted July 30, 2004

Abstract. Phase pure lanthanum substituted bismuth titanate was prepared by an aqueous solution-gel route. In this route aqueous precursors are synthesized by stabilization of the metal ion in the aqueous medium through complexation with strong electron donor ligands. The chemical structure of metal-less, monometal ion as well as multimetal ion precursorgels was studied by means of FTIR and FT-Raman spectrometry. The precursors were transformed to phase pure oxides by heat treatment in an appropriate dynamic atmosphere. The decomposition reactions of the gels were studied by means of several hyphenated thermal analysis techniques (thermogravimetry coupled on-line to FTIR or MS (TGA-MS, TGA-FTIR) and high temperature—diffuse reflectance infrared spectrometry by fourier transform (HT-DRIFT)) and reactions are proposed. The phase formation was studied by means of X-ray diffraction. Phase segregation during gel calcination was correlated to the oxygen partial pressure. An explanation for this phenomenon was suggested based on thermal analysis and on SEM and TEM studies.

Keywords: aqueous solution-gel, gel structure, decomposition pathway, oxide crystallization, hyphenated thermal analysis

1. Introduction

Bismuth titanate ($Bi_4Ti_3O_{12}$, BiT) has a layer-structured perovskite lattice, consisting of $Bi_2O_2^{2+}$ layers interleaved with $Bi_2Ti_3O_{10}^{2-}$ perovskite layers, which is called the Aurivillius structure. These layers are stacked consecutively along the *c*-axis. It has an orthorhombic unit cell [1] with monoclinic distortion [2]. BiT is a ferroelectric material, for which there is a lot of interest recently due to its possible application in ferroelectric random access memories (FRAMs), which are non-volatile. In order to improve its fatigue resistance, the Bi^{3+} is partially substituted by La^{3+} to form BLT ($Bi_{4-x}La_xTi_3O_{12}$) [3].

In our laboratory several aqueous precursor solutions for the synthesis of BiT as well as BLT powders and thin films have been developed [4–6]. Like other sol–gel methods, the aqueous solution-gel method aims to mix the metal ions most intimately possible, by synthesis of stable, aqueous multimetal ion solutions. Transforming the solutions into amorphous and homogeneous gels, by evaporation of the water, fixates the homogeneity. This high degree of homogeneity in the precursor phase allows a lower crystallization temperature of the desired oxide phase, compared to traditional solid-state routes. An aqueous route has specific advantages over alcoholic sol–gel routes. The starting products, which

*To whom all correspondence should be addressed.

are simple salts like citrates and acetates, do not need to be protected from the ambient moisture and are less expensive than metal alkoxides and alkoxyalcohols. Since there are no organic solvents used, associated health and ecological risks are considered to be smaller. However, since the high-valent metal ions are very sensitive to hydrolysis, a critical issue to be overcome is their stabilization to prevent reaction with the H_2O, which would lead to precipitation and thus phase segregation. In our laboratory this issue has been solved by complexation of the metal ions with appropriate strong electron donors, such as citric acid and hydrogen peroxide [7–10] and monoethanolamine [6].

Even though nanoscale-homogeneous precursors for BLT were prepared [6], still a mixture of Aurivillius and Sillenite phases was formed after thermo-oxidative decomposition in a furnace. Nonetheless, an *in-situ* study of the phase formation with high temperature XRD proved that it was indeed possible to obtain phase pure BLT from our precursor [6], but that there was a need for an optimization. To this purpose statistically designed experiments were used successfully [11]. From these experiments it was concluded that the oxygen partial pressure during gel thermolysis was the most important factor correlated with phase segregation of Sillenite ($Bi_{12}TiO_{20}$). This also explained the discrepancy between the HT-XRD and furnace result.

So, the phase segregation was suspected to be related to processes occurring during gel thermolysis, the stage at which the pO_2 has the strongest influence. It was therefore considered very important to understand the gel's decomposition mechanism, in order to understand the pO_2 dominated phase segregation. However, in order to unravel the gel's decomposition, it is of great importance to understand its structure first. In this paper the results of studies with this purpose are described. Furthermore, the structure and thermal behavior of monometal ion gels, containing only one of the constituent metal ions of BLT, was studied as well. In this way the behavior of the BLT gel could be compared with and related to the monometal ion gels' behavior.

2. Experimental Details

2.1. Precursor Synthesis

The BLT precursor was synthesized according to the procedure which has been described in detail in a previous paper [6]. First, precursors were prepared for all three metal ions separately. For Bi^{3+} and La^{3+} the starting products are citrate salts, which are dissolved by addition of ammonia and monoethanolamine. The precursor for Ti^{4+} is a citratoperoxotitanate (IV) complex with high solubility and stability in water [10]. A solution of this complex is synthesized in the following manner. First an appropriate amount of $Ti(OPr^i)_4$ is hydrolyzed in water. A precipitate is formed immediately, due to hydrolysis and condensation reactions. This precipitate is filtered and washed with plenty of water. Citric acid in a molar ratio of 2:1 and H_2O_2 in a molar ratio of 1.1:1 against Ti^{4+} are added to the wet precipitate and the mixture is heated to 60°C. This results in the formation of a clear solution. Subsequently, an aqueous solution of NH_3 is used to increase the pH to 7. The starting product in our case is a metal alkoxide, but it is one of the least expensive. It was even slightly less expensive than metallic Ti powder used by Kakihana et al. [15] as a starting product for the synthesis of the water soluble ammonium citratoperoxotitanate (IV) complex $(NH_4)_8[Ti_4(C_6H_4O_7)_4(O_2)_4]\cdot 8H_2O$.

After exact determination of their concentration (ICP-AES, Perkin Elmer, Optima 3000), the monometal ion solutions are mixed together in any desired stoichiometry, without further pH adjustment, in order to obtain the BLT precursor solution ($pH \approx 7$). In this study the composition $Bi_{3.5}La_{0.5}Ti_3O_{12}$ was chosen for its relevance in FeRAM applications.

Glassy, XRD amorphous gels are obtained by evaporation of the monometal ion and BLT solutions in an air-flushed furnace at 60°C. The Bi^{3+} solution is prone to precipitation during gelation. However, it was possible to obtain a homogeneous, amorphous gel by using an increased citrate:Bi^{3+} ratio (2:1) at a pH of 7.

Furthermore, "metal-less" gels were prepared in an air-flushed furnace at 60°C, by evaporation of an ammonium citrate solution ($pH = 7$) and an ammonium citrate solution containing ethanolamine ($pH = 7$; molar ratio of citric acid to ethanolamine 1.5:1 as in the BLT solution), which will be referred to as the ETA-ammonium citrate gel.

2.2. Characterization Techniques

The chemical structure of the amorphous precursor gels was studied by means of fourier transform Raman and infrared spectrometry (FTIR Bruker IFS66, combined with a FRA106 FT-Raman spectrometer equipped with a Nd-YAG laser of 1064 nm). Spectra were collected with a resolution of 4 cm^{-1}.

The thermo-oxidative decomposition pathway was studied by several hyphenated (i.e. coupled) thermal analysis techniques in a dynamic atmosphere. To study the gases evolved during gel thermolysis, thermogravimetric analysis (TGA, TA Instruments TGA 951-2000) coupled on-line to a FTIR spectrometer (Bruker IFS48) or a quadrupole mass spectrometer (MS, Thermolab VG Fisons) was used [12]. The latter is used with 20 eV ionization energy to avoid fragmentation of H_2O ($m/z = 18$) into OH ($m/z = 17$), hereby enabling the detection of NH_3 ($m/z = 17$) without interference. Complementary to the TGA-EGA (evolved gas analysis), high temperature—diffuse reflection fourier transform infrared spectrometry (HT-DRIFT, Bruker IFS66) was used for *in-situ* tracking of changes in the solid phase during the heat treatment. The equipment can only be used up to 400°C in an oxidative ambient. In order to study the chemical structure of the solid phase at temperatures >400°C, the gel was heated in a TGA furnace, quenched and a DRIFT spectrum was recorded at room temperature afterwards.

An *in-situ* study of phase formation during heat treatment in static air, was carried out using high temperature XRD (HT-XRD, Siemens D-5000, equipped with Göbel mirror, Pt heating stage (HTK 10, Anton Paar) and PSD (mBraun), Cu Kα). X-ray diffraction patterns at room temperature were recorded on the same diffractometer, using a standard Silicon sample stage.

Scanning electron micrographs of powders, prepared by heating the gel up to the desired temperature and in the atmosphere of choice in the TGA furnace, were obtained on a Philips XL30-FEG SEM equipped with an energy dispersive X-ray detector (EDX) with a super ultra thin window. Transmission Electron Micrographs (Philips CM12) were taken from similarly prepared powders, after ultrasonic dispersion in methanol and picking up on a formvar grid.

3. Results and Discussion

3.1. Precursor Gel Structure

FTIR and FT-Raman (Fig. 1(A) and (B)) spectra of metal-less, monometal ion and BLT gels were recorded. The spectrum of the ammonium citrate gel is practically identical to that of the ETA-ammonium citrate gel.

The FTIR spectra of all of the gels show similar features. The extremely broad band from 3730 to 2250 cm^{-1} can be ascribed to O—H, N—H and C—H stretching vibrations, broadened due to extensive hydrogen bonding. In some of the spectra a shoulder at ~1710 cm^{-1} is present, which is ascribed to the carbonyl stretching vibration of free citric acid. It could have formed from ammonium citrate by loss of ammonia during gel formation at 60°C. Around 1580 and 1400 cm^{-1} respectively the asymmetric and symmetric stretching of a carboxylate group are found. The Δ value ($\Delta = \bar{\upsilon}_{as} - \bar{\upsilon}_s$) of 180 cm^{-1} could indicate the presence of bridging carboxylate metal ion complexes

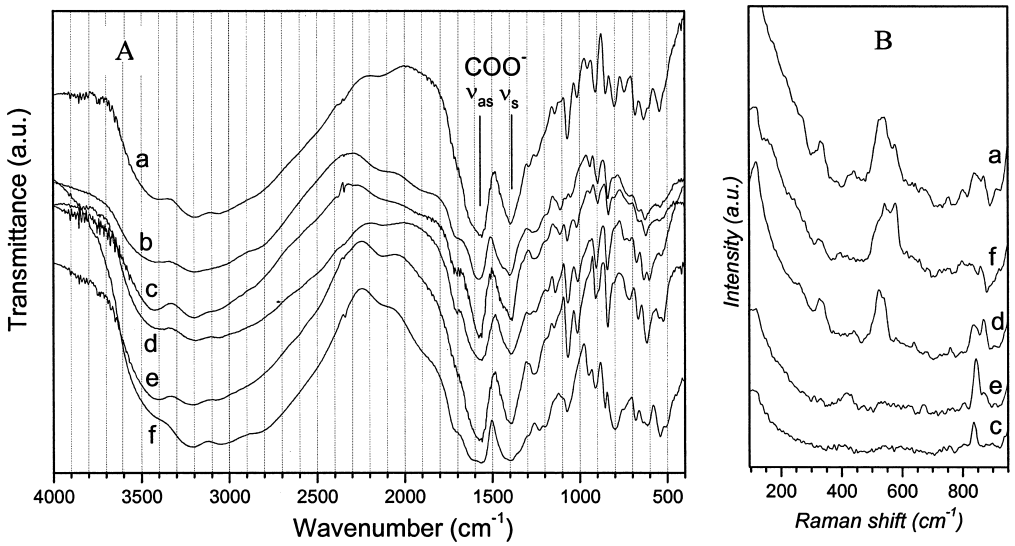

Figure 1. (A) FTIR and (B) FT-Raman spectra of (a) BLT gel; (b) ammonium citrate gel; (c) ETA-ammonium citrate gel; (d) Bi^{3+} gel; (e) La^{3+} gel; and (f) Ti^{4+} gel.

in all of these gels [13]. It is however also possible that the bonding is ionic, since the Δ values for bridging complexes are close to the values for ionic bonds. This is illustrated by a comparison with the metal-less gel's FTIR spectrum: it contains only ionic bonded carboxylates such as NH_4^+-OOC, but has a similar Δ value. For the Ti^{4+}-gel the carboxylate bands are broad, which makes it difficult to conclude about the type of coordination. The band at 1250 cm^{-1} can be ascribed to the ν(C—O) of the –COOH or to a CH_2 wagging vibration. The band at $\sim$1070 cm^{-1} is ascribed to the alcoholic or alkoxide C—O stretching vibration, ν(C—O) [13]. From the analogy between the vibrational spectra it is clear that the M^{n+}-gels have structures very similar to the structure of the metal-less gels. It is concluded that the citrate gels contain metal ion carboxylate complexes and ammonium citrate molecules. Cross-linking, leading to the formation of a three dimensional gel network, is present by ionic NH_4^+-O bridges and possibly also ionic metal carboxylate bonds [14]. It is also possible, in agreement with the Δ values given above, that some of the citrate groups bridge two metal ion centers in the gel, as is the case in the structure of the crystalline citratoperoxo-Ti (IV) complex described by Kakihana et al. [15].

To obtain information on the metal ion complexes themselves, the wavenumber region below 1000 cm^{-1} is the most interesting, since vibrations of bonds involving metal ions are expected here.

The FTIR spectra of the Ti^{4+}-gel as well as the BLT gel are characterized by three bands at 800, 540 and 505 cm^{-1} which can be ascribed to the coordinated peroxogroup ($\nu(O_2)$, $\nu_a(MO_2)$ and $\nu_s(MO_2)$) [16, 17]. These bands can also be distinguished in the Raman spectra, although the intensity at 800 cm^{-1} is low. Detailed information on the Ti^{4+} species was obtained from the crystalline complex, which precipitated starting from a highly concentrated Ti^{4+} solution. This complex was characterized by means of XRD and it was concluded that it is identical to the citratoperoxotitanate (IV) described by Kakihana et al. [15]. This is a tetranuclear metal ion complex, consisting of two binuclear fragments interlinked through a bridging carboxylate group [15]. The peroxo group coordinates to the Ti^{4+} in a triangular bidentate manner (side-on) [15]. The citrate acts as a tridentate ligand, coordinating to the metal ion via two carboxylate groups and the deprotonated alcoholic oxygen [15]. There are two non-coordinated carboxylate groups present in the complex [15]. The latter are important for the synthesis of an amorphous gel starting from the Ti^{4+} precursor solution, due to the fact that they are available for making the cross-links between complexes by means of ionic NH_4^+-$^-$O bridges. Other factors determinant for the gelation of the aqueous metal chelate solutions are the presence of an excess of citric acid to favour the complexation equilibrium and the fast evaporation in a furnace, which leads to a fast increase of the solution's viscosity, preventing long range ordering and precipitation.

The Bi^{3+} gel's Raman spectrum is characterized by bands at $\sim$330, 440 and 530 cm^{-1}. The La^{3+} gel has a Raman band at 420 cm^{-1}. The metal-less gel shows no bands at any of these positions. Therefore they are ascribed to M-N and M-O stretches [17, 19]. The Bi^{3+} and La^{3+} gels possibly contain mixed ligand complexes with citric acid and ethanolamine. Ethanolamine is a known bidentate ligand, which coordinates metal ions with the amine nitrogen and alcoholic oxygen, hereby forming a stable 5-membered chelate ring, with its hydroxyl group either deprotonated or protonated [18, 20, 21]. It was observed that it is only possible to obtain the La^{3+} solution by addition of ethanolamine. With the addition of ammonia alone this is impossible at the same pH. Furthermore, ethanolamine is necessary to stabilize the Bi^{3+} precursor solution against precipitation [6]. Based on these observations and on the FTIR and Raman spectra, it is suggested that both the ethanolamine and the citrate are coordinated to the Bi^{3+} and La^{3+}.

The BLT spectrum can be considered to be a result of the overlap of the monometal ion gel spectra. The BLT gel may consist of a mixture of the monometal ion complexes homogeneously distributed and cross-linked into a matrix of ammonium citrates. However, the presence of heterometallic complexes could not be excluded.

3.2. Gel Decomposition Mechanism

The precursor gels are subjected to thermal treatment in order to decompose the organic components and obtain the crystalline oxide. In order to prepare a homogeneous, phase pure oxide, it is very important that the small-scale mixing of the multimetal ion gels is retained during gel thermolysis.

The thermo-oxidative decomposition of the gels was studied by means of TGA (10°C/min, 100 ml/min dry air) as shown in Fig. 2(A). The gel decomposition can be divided in several major regions with increased reaction rates, which will be referred to as "steps" (Table 1).

Table 1. Overview of TGA-results at 10°C/min in dry air (100 ml/min), division into several regions.

Gel	Step 1	Step 2	Step 3	Step 4	Step 5
ETA-NH_4^+-citrate	160–310°C	350–475°C	475 –680°C		
Bi^{3+}	160–260°C	260–325°C	445–510°C		
La^{3+}	160–250°C & 250–310°C	310–425°C	425–500°C	550–660°C	660–725°C
Ti^{4+}	120–260°C	300–400°C	400–500°C	500–595°C	
BLT	150–260°C	260–415°C	415–510°C		

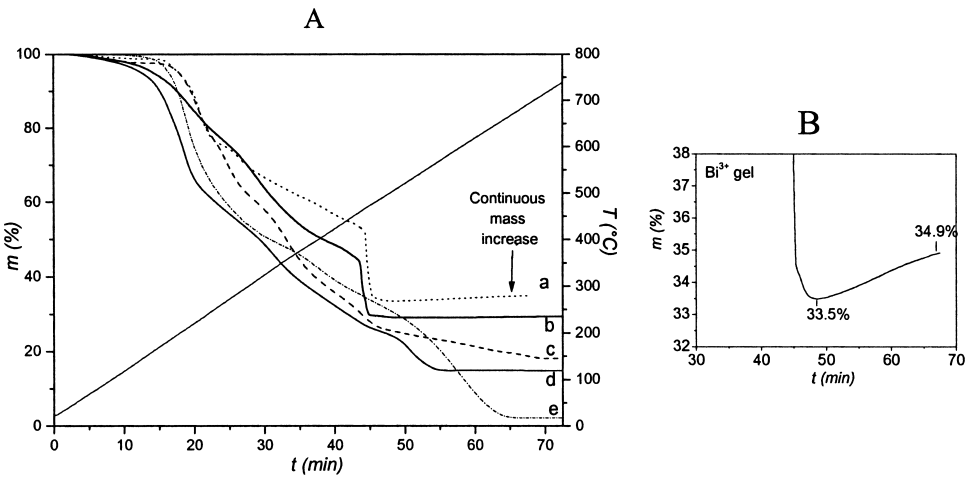

Figure 2. (A) TGA at 10°C/min in 100 ml/min dry air of (a) Bi^{3+} gel (. . .), (b) BLT gel (–), (c) La^{3+}-gel (- - -), (d) Ti^{4+}-gel (-..-..) and (e) ETA-ammonium citrate gel (_.-._.-._); (B) Enlargement of the Bi^{3+} gel's TG curve to clarify the continuous mass increase after the final decomposition step.

Only for the Bi^{3+}-gel a continuous mass increase is observed at temperatures above 490°C. This is clearly seen in Fig. 2(B), which shows the relevant part of the Bi^{3+} gel's TG curve enlarged.

Evolved gases were detected by FTIR or mass spectrometry during heating of the gels. (HT-)DRIFT measurements were carried out to study the structural changes in the solid phase during gel thermolysis.

3.2.1. Decomposition of the Metal-Less Gel. The decomposition pathway of a metal-less gel was studied for comparison with the gels containing metal ion(s). Ammonium citrate decomposition has been described by Van Werde et al. [8].

The complexity of the metal-less ETA-ammonium citrate gel decomposition indicates the occurrence of different types of chemical reactions. At a relatively low temperature (around 200°C) uncomplexed ammonium citrate decomposes with the release of several volatile species such as ammonia, water, carbon dioxide and decomposition products of citric acid ($m/z = 68$ [4]), due to reaction (1) and continued reaction (e.g. reaction 2) of the citric acid formed.

$$NH_4OOC{-} \rightarrow NH_3 + HOOC{-} \quad (1)$$

$$RCOOH \rightarrow RH + CO_2 \quad (2)$$

However, in contrast to this metal-less gel, citric acid itself is completely decomposed around 220°C at 10°C/min, with subsequent formation of aconitic acid, itaconic and citraconic acid and anhydride [4, 22]. Other reactions besides (1) and (2) must therefore occur. A possible reaction is the formation of amides by dehydration of the ammoniumcarboxylate (3). At higher temperatures these amides could decompose further into ammonia and carboxylic acids or dehydrate into nitriles (reactions 4 and 5). Another mechanism, which is not yet well understood, enables the formation of hydrogen cyanide [23]. Possible further dehydration and decarboxylation reactions of the carboxylic acids

are (6) and (2).

$$NH_4OOC{-} \rightarrow {-}CONH_2 + H_2O \quad (3)$$

$$R{-}CONH_2 + H_2O \rightarrow R{-}COOH + NH_3 \quad (4)$$

$$R{-}CONH_2 \rightarrow R{-}CN + H_2O \quad (5)$$

$$R{-}CH_2{-}COOH \rightarrow R{-}CH{=}C{=}O + H_2O \quad (6)$$

The occurrence of these reactions was supported by the observations made in the hyphenated thermal analysis. In Tables 2 and 3 an overview and summary per decomposition step of the evolved gases observed in TGA-FTIR and/or –MS is given. The spectra and traces as a function of time are not shown themselves in order not to overload with figures. The (HT-)DRIFT spectra at selected temperatures are shown in Fig. 3.

The first decomposition region is characterized by the evolution of mainly H_2O and NH_3, which is explained by reactions 1, and possibly also 3 and 4. At the same time in the HT-DRIFT the peaks at 1710 and 1250 cm^{-1} (which also shifts to lower wavenumber) become stronger due to the formation of carboxylic acid (reaction 1). The evolution of carbon dioxide, which is present throughout the entire decomposition, also starts in the low temperature region. This is ascribed to the decarboxylation of carboxylic acid in this temperature region (reaction 2). Immediately these reactions are followed by the evolution of m/z 68, which is an indicator for the decomposition of citric acid [4]. In HT-DRIFT a shoulder at 1765 cm^{-1} appears, which could indicate the formation of unsaturated cyclic anhydrides, decomposition products of citric acid, if the expected peak at 1850 cm^{-1} is considered too weak to be detected.

The second decomposition region is characterized by the detection in TGA-MS of CH_3^+ ($m/z = 15$) and CH_3CN^+ ($m/z = 41$), which could be explained by mechanism (5), as well as by the start of the evolution of hydrogen cyanide ($m/z = 27$) and CO_2 ($m/z = 44$), the latter possibly formed in reaction (2), but probably mostly produced in combustion reactions involving ambient O_2. Another evolved compound possibly formed through a combustion reaction is H_2O. CO could have been formed by partial oxidation of the organic compounds or by pyrolysis. In TGA-FTIR an absorption peak at 3015 cm^{-1} is detected, typical of unsaturated compounds which may have been formed by dehydration reactions. A small amount of ketene ($CH_2{=}C{=}O$, $m/z = 42$) was detected in TGA-MS at the end of step 1 and during steps 2 and 3, which supports the occurrence of reaction (6).

Table 2. Peak assignment of mass fragments or IR bands in TGA–MS or TGA–FTIR of the gels.

Product or mass fragment	M/z detected in TGA-MS	Wavenumber of absorption in TGA-FTIR (cm^{-1})
NH_3	17	3330, 1623, 964, 930
H_2O	18	
CO_2	44	3715, 3615, 2330, 667
HCN	26, 27	3275, 3335
$R{-}C{\equiv}N$	41 (CH_3CN)	2250
CO		2175, 2110
CH_3^+	15	2930
Decomposition products of citric acid	68 ($C_4H_4O^+$, cyclic anhydrides) 55 ($C_3H_3O^+$, $CH_2{=}CH{-}C{\equiv}O^+$, typical for citraconic anhydride and itaconic acid)	1730 (α-β unsaturated carboxylate e.g. aconitic acid)
Decomposition product of ammonium citrate	111 ($C_5H_5NO_2$, 3-Methyl-maleimide)	
Unsaturated organics		3015 (ν(H–C=))
NO	30	
Saturated organics		2920 (ν(H–C–))
Ethanolamine	30 ($CH_2NH_2^+$)	2880 and 2940

Table 3. Summary of evolving gases detected in TGA-MS and TGA-FTIR (10°C/min, 100 ml/min dry air) ordered per gel and per decomposition step.

Step	ETA-ammonium- citrate gel	Bi^{3+}-gel	La^{3+}-gel	Ti^{4+}-gel	BLT gel
1	NH_3 H_2O CO_2 CH_3CN CH_3^+ $C_4H_4O^+$	NH_3 H_2O CO_2 $C_4H_4O^+$ $C_3H_3O^+$ Aconitic acid 3-Methyl-maleimide Ethanolamine (30)	NH_3 H_2O CO_2 CH_3^+ $C_3H_3O^+$ Aconitic acid 3-Methyl-maleimide Ethanolamine (30)	NH_3 H_2O CO_2 CH_3^+ $C_4H_4O^+$ 3-Methyl-maleimide	NH_3 H_2O CO_2
2	H_2O CO_2 CH_3CN CH_3^+ $C_4H_4O^+$ Start of evolution of HCN CO H—C= CH_2=C=O	H_2O CO_2 $C_4H_4O^+$ CO	NH_3 H_2O CO_2 CH_3CN CH_3^+ CO	H_2O CO_2 CH_3CN HCN CO	H_2O CO_2 CH_3CN CH_3^+ $C_4H_4O^+$ CO
3	H_2O CO HCN H—C= CO_2 CH_3^+ (small amount) CH_3CN (small amount) CH_2=C=O	NH_3 H_2O CO HCN H—C= CO_2 CH_3^+ CH_3CN NO	NH_3 H_2O CO_2 CH_3^+ CH_3CN NO	CO HCN CO_2	NH_3 H_2O CO H—C= CO_2 CH_3^+ CH_3CN NO
4	/	/	CO_2 NO	CO_2 NO H_2O CO HCN	/
5	/	/	CO_2	/	/

During the final decomposition step the evolution of CO, CO_2 and HCN was seen. This reaction is considered to be a combustion. The formation of CO is caused by the oxygen deficit, due to the high rate of the O_2 consuming reactions. This is observed in TGA-MS as a drop of the intensity of $m/z = 32$ (O_2) below the background value of dry air. During both step 2 and 3 the evolution of nitriles is observed in TGA-MS (CH_3CN^+) and TGA-FTIR (2250 cm^{-1}, reaction (5)). Supporting evidence was found in the DRIFT spectra of the gel: after heating up to 475 and 600°C a nitrile absorption peak at 2220 cm^{-1} was detected. Above 680°C the gel has decomposed completely, as is seen from the TGA (Fig. 2(A)).

3.2.2. Decomposition of the M^{n+} and BLT Gels. Based on Section 3.1, the (mono)metal ion gels are considered to be built from metal ion complexes, which are bonded to an organic backbone, consisting of citrate ions cross-linked by the (ethanol)ammonium counterions. They have a structure similar to that of the metal-less gel. Therefore, it is understandable that these gels' decomposition showed strong analogies with that of the metal-less gel (vide infra). Differences between the

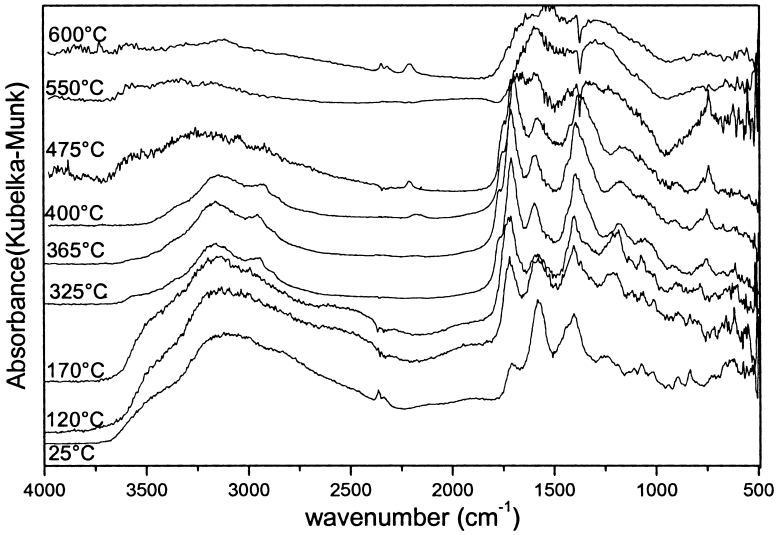

Figure 3. (HT-)DRIFT of the metal-less ETA-ammoniumcitrate gel (10°C/min, 100 ml/min dry air).

decomposition pathways of the different mono- and/or multimetal ion gels are due to differences in the nature of the metal ions and the complexes they formed, and to reactions they can undergo with the evolved gases, as will be explained below.

In general the decomposition consists of several "steps", which by overlapping make the decomposition very gradual. Another reason for the graduality of the decomposition could be the transportation of reaction products out the dense gel pieces. The most important decomposition products detected in TGA-MS and –FTIR are assigned in Table 2 and summarized per decomposition step and per gel in Table 3. The (HT-)DRIFT spectra at selected temperatures are shown in Fig. 4 for the four gels.

In a first step, at relatively low temperatures, the decomposition is similar to that of the metal-less gel, which supports the hypothesis that uncomplexed organic compounds are decomposing in this temperature range. So, the free (ethanol)ammonium citrate decomposes by the reactions described in Section 3.2.1, leading to the evolution of water, NH_3 and decomposition products of citric acid such as CO_2, aconitic acid and cyclic anhydrides (peak at 1730 cm^{-1} in TGA-FTIR; CH_3^+, $C_4H_4O^+$ and $C_3H_3O^+$ in TGA-MS [4]). For the Bi^{3+}- and La^{3+}-gels $m/z = 30$ was detected with TGA-MS during the first decomposition step, which indicates the evolution of ethanolamine. In HT-DRIFT (Fig. 4) a decrease of the intensity between 3500 and 2500 cm^{-1} (ν(N—H), ν(O—H)) is seen correspondingly. This also enables the detection of ν(—C—H) around 2920 cm^{-1}. At the same time the intensity at 1720 cm^{-1} increases, which signalizes the formation of carboxylic acids. At slightly higher temperatures small peaks around 1840 (very weak) and 1775 cm^{-1} (medium) are seen, which are ascribed to the formation of cyclic anhydrides. Furthermore, for the Ti^{4+}- and BLT gel the intensity around 1660 cm^{-1} clearly becomes stronger, which could be due to the formation of amides (ν(C═O)). For all the monometal ion gels 3-methyl-maleimide ($m/z = 111$) was detected, which supports the possibility of amide formation [4]. The metal ion complexes are not expected to experience large changes in this temperature range.

In the second step, at higher temperatures, the coordination with the ligands destabilizes and the originally coordinating groups are decomposed, leading to the evolution of similar gaseous reaction products as seen in the first step (mainly CO_2 and H_2O). An indicator for this process is the disappearance of the C—O(—M or H) stretching vibration at 1080 cm^{-1} from the HT-DRIFT spectrum at the end of the second step [4, 8]. The formation of metal oxides now becomes possible. At the same time, partial decomposition of the amides and other organic backbone decomposition intermediates, is observed (CH_3CN, HCN, CO and H—C═). Differences in the gas evolution temperature are seen for the different gels, which probably is due to the influence of the metal ion.

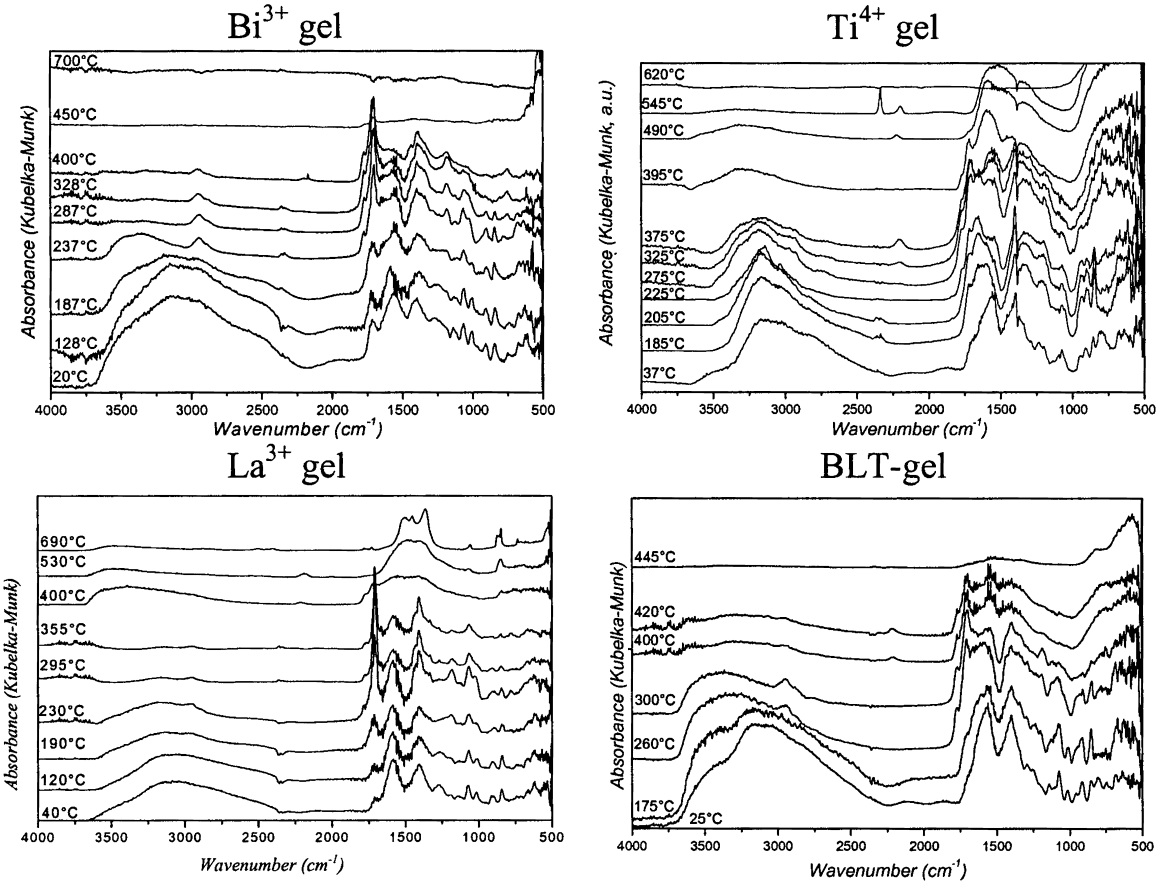

Figure 4. (HT-)DRIFT spectra of the Bi^{3+}-, La^{3+}-, Ti^{4+}- and BLT-citrate gels (10°C/min, 100 ml/min dry air).

In the subsequent step(s) all of the nitrogen containing organic matter which is still left in the powders is removed completely, leaving only the oxide(s) behind. This is accompanied by the detection of NO, CH_3^+, HCN, CO, CO_2, H_2O, NH_3, CH_3CN^+ and unsaturated organic compounds (peak at 3012 cm^{-1} in TGA-FTIR) and also by the continued decrease of the absorbance in the HT-DRIFT spectra over the entire wavenumber range from 4000 to 1000 cm^{-1}. For the La^{3+} gel a reaction with $CO_{2(g)}$ was observed in the DRIFT measurement. It leads to the formation of dioxymonocarbonates ($La_2O_2CO_3$) of type I at 530°C and type IA at 690°C (detail in Fig. 5, with assignment of the carbonate vibration modes in accordance with Turcotte et al. [24]). As a side effect this also leads to the extension of the decomposition up to much higher temperatures.

In view of the types of evolving species and the presence of anatase TiO_2 at 525°C (evident from Fig. 7) it is concluded that the formation of an (oxy)carbonate is not the reason for the occurrence of a fourth step in the decomposition of the Ti^{4+}-gel.

3.3. *In-Situ Study of the Phase Formation*

The phase formation was studied *in-situ* by means of high-temperature XRD in static air (10°C/min). Series of diffraction patterns were recorded at increasing temperatures. Pt peaks are caused by the sample holder.

A HT-XRD measurement of the Bi^{3+}-gel (Fig. (6A)) showed that the crystallization starts between 350 and 375°C already, with formation of a phase that agrees well with metastable β-Bi_2O_3 [25, 26] (JCPDS 27-0050 [27]). Between 450 and 725°C a second bismuth oxide phase is distinguished, which could be identified as α-Bi_2O_3 (JCPDS 41-1449). Between 725 and 750°C an abrupt phase transformation to a mixture of

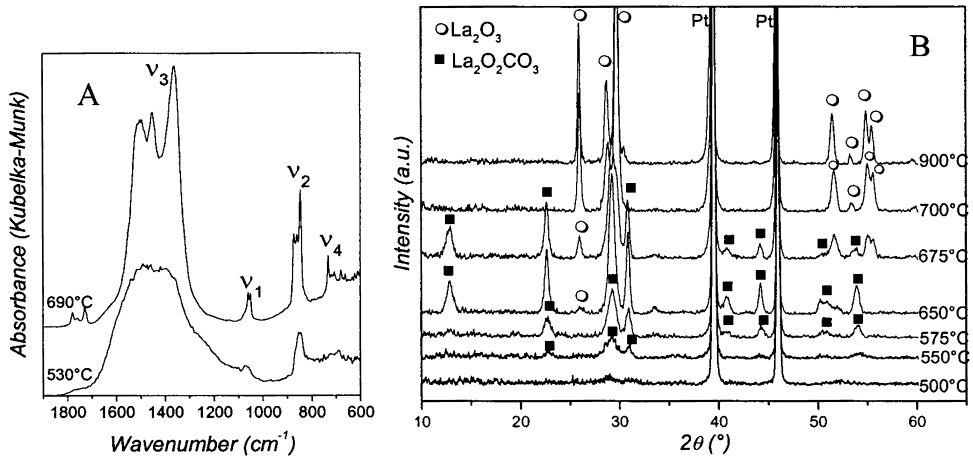

Figure 5. (A) DRIFT spectrum of the dioxymonocarbonate intermediates formed by heating the La^{3+} gel to 530 (type I) and 690°C (type IA) in a TGA furnace at 10°C/min in 100 ml/min dry air and (B) HT-XRD measurement of the La^{3+} gel (static air, 10°C/min).

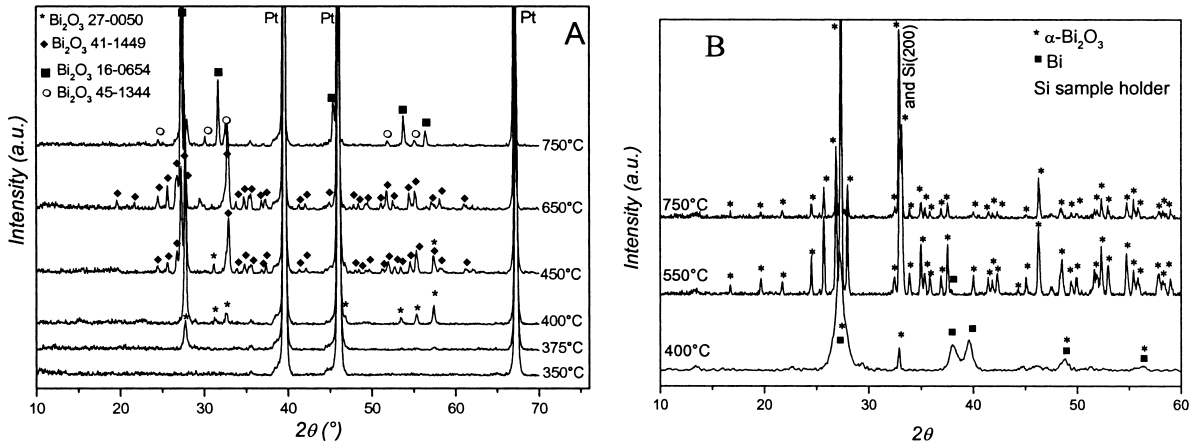

Figure 6. (A) HT-XRD measurement of the Bi^{3+} citrate gel (static air, 10°C/min), (B) XRD patterns at room temperature of a Bi^{3+}-gel heated in a TGA furnace to the temperatures indicated (10°C/min, 50 ml/min dry air).

a metastable γ-Bi_2O_3 (JCPDS 45-1344) and a face centered cubic Bi_2O_3 phase (JCPDS 16-0654) occurs. Based on visual inspection of samples obtained by heating this gel, metallic bismuth was suspected to be present as well. Metallic bismuth was not observed in the HT-XRD, which is due to its low melting point (T_m = 271.4°C). For this reason XRD patterns (Fig. 6(B)) were recorded at room temperature using a Si sample holder. The samples were prepared by heating of the gel in a TGA furnace up to 400, 550 and 750°C (10°C/min, 50 ml/min dry air). It is clearly found that at 400 and 550°C the metallic form is present besides α-Bi_2O_3. Upon cooling the α-phase is always formed [25, 26], which explains the difference between our HT-XRD and XRD's at room temperature. The Bi^{3+} was probably reduced to metallic Bi by the organic material directly or by the carbon monoxide, which is evolved during the second and final decomposition step. This was not observed for La^{3+} and Ti^{4+} since these have much lower reduction potentials. Metallic bismuth has disappeared from the room temperature diffractogram of a powder prepared at 750°C, most probably due to oxidation by the ambient O_2. The oxidation of metallic Bi to the oxide explains the occurrence of the increase in mass, seen in the TGA above 490°C (Fig. 2(B)).

The crystallization of type I $La_2O_2CO_3$ (JCPDS 23-0320) from the La^{3+}-gel has occurred at 550°C, as shown by the HT-XRD results (Fig. 5(B)). This agrees with the HT-DRIFT measurement. Starting from 650°C a diffraction peak appears at 26.2°2θ, which indicates the start of the dioxymonocarbonate's decomposition to lanthanum oxide (La_2O_3, JCPDS 05-0602). At 700°C and above the dioxymonocarbonate is completely decomposed and phase pure La_2O_3 is formed. Type IA lanthanum dioxymonocarbonate (JCPDS 23-0322.) was not observed in HT-XRD in contrast to HT-DRIFT, which is ascribed to differences in sample amount and heating rate, which have a strong influence on the transformation of type I to type IA dioxymonocarbonate, according to the findings of Turcotte et al. [24].

The HT-XRD measurement of the Ti^{4+}-gel (Fig. 7) demonstrated that the crystallization starts between 500 and 525°C with the formation of anatase TiO_2 (JCPDS 21-1272). Between 575 and 600°C the Anatase starts to transform to the Rutile phase (JCPDS 21-1276). Starting from 775°C phase pure Rutile TiO_2 is present.

For the BLT gel a HT-XRD has been published elsewhere [6]. It was shown that starting from 525°C immediately the desired Aurivillius phase crystallizes, without the formation of any intermediate or secondary phases.

It is clearly concluded, by comparison of the TGA results (Fig. 2(A)) and the HT-XRD results (Fig. 5(B), 6(A) and 7), that for all of the monometal ion gels crystallization occurs at temperatures below the completion of the final decomposition step. This indicates that the metal ion complexes have decomposed completely, even though the entire carbon-containing fraction has not been removed. For the BLT gel the opposite was true, as we reported earlier [6]. Here the oxide crystallizes only after the final decomposition step has taken place. From a comparison of the crystallization temperatures of the monometal ion and BLT gels, it is clear that Bi^{3+} would be expected to cause phase segregation due to its gel's much lower crystallization temperature [28]. Nonetheless this was not observed in the HT-XRD experiment on the BLT gel, as reported earlier [6]. At first sight, this might also be attributable to the low melting point of metallic bismuth, which can hypothetically form as a secondary phase and remain undetected with HT-XRD. However, in this case an oxidized bismuth rich secondary phase would imperatively be present in the HT-XRD patterns at higher temperatures due to oxidation of the metallic bismuth. Since this was not observed, metallic bismuth formation most probably does not occur during the HT-XRD measurement of the BLT gel.

3.4. *Influence of the Oxygen Partial Pressure on Gel Thermolysis*

Due to the important effect of the oxygen partial pressure on the phase purity of the oxide, the thermo-oxidative decomposition of the gel was studied at 5, 10, 20, 50, 75 and 100% (vol) O_2 in N_2. The gel was heated at 20°C/min up to 625°C followed by an isothermal period of 55 minutes and the gas flow rate was set to 15 ml/min. The thermograms are shown in Fig. 8.

The decomposition always occurred through the same number of steps. The first decomposition step is the same in all of the ambient compositions. However,

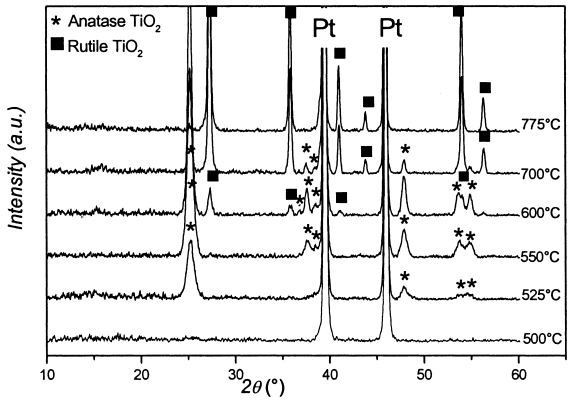

Figure 7. HT-XRD measurement of the citratoperoxo-Ti(IV) gel (static air, 10°C/min).

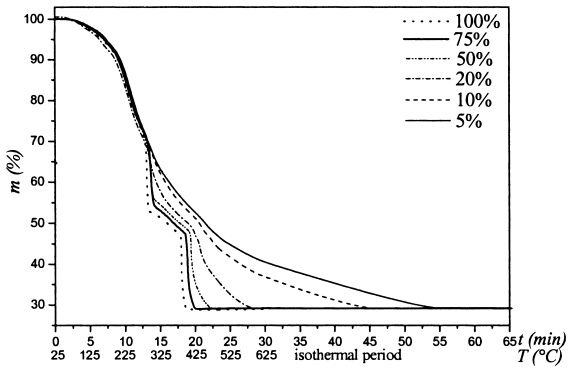

Figure 8. TGA of the BLT gel as a function of %(vol)O_2 (20°C/min, 15 ml/min).

it is clear that the reaction rates of the second and third step increase with the %(vol) O_2. This is understandable since O_2 is one of the reactants, so an increase of its concentration will cause an increase of the reaction rate. The exothermic nature of these reactions will lead to an increase of the actual sample temperature above the programmed one, which is higher with higher pO_2. In turn this will accelerate the combustion reaction more. The reaction slows down when all the material, which is susceptible to decomposition in the specific temperature region, is combusted (either formerly complexing organic material (step 2) or the organic rest fraction (step 3 etc.)).

These observations confirm that, in the low temperature region, the O_2 independent decarboxylation and dehydration of the uncomplexed ammonium citrate occur. However, at higher temperatures oxygen plays an important part in the steps occurring.

It was found that only in dry air phase pure Aurivillius structured $(Bi,La)_4Ti_3O_{12}$ was formed, while in all other cases $Bi_{12}TiO_{20}$ was seen as well, as we reported earlier [11].

From Fig. 8 it can be concluded that when a phase pure product is formed, which occurs only in 20% (vol) oxygen [11], the second decomposition step, which is the release of the ligands from the metal ions, occurs rather gradually, while the final decomposition step occurs abruptly. Indeed, if the second step occurs abruptly, as is the case in 100, 75 and 50% O_2, and if the third step occurs too gradually and is still going on during the isothermal period, as is the case in 5 and 10% O_2, the secondary Sillenite phase is formed, see also [11].

3.5. *Electron Microscopic Study of the Phase Segregation*

In order to find out at which time during the gel thermolysis in oxygen the phase segregation of the Sillenite occurs, the BLT gel was heated in the TGA-furnace at 5°C/min in 15 ml/min O_2 or dry air up to different temperatures (e.g. 200, 300, 450°C) chosen according to the thermogram (Fig. 9) and quenched or heated up to 750°C followed by an isothermal period of 20 minutes. The resulting powders were characterized by means of FTIR (Fig. 10) and their microstructure and chemical composition was studied by means of scanning electron microscopy (Figs. 11 and 12). In order to study the temperature interval between 300 and 400°C more carefully, a TEM study was carried out on powders heated in 15 ml/min oxygen at 5°C/min up to 310, 350 and 375°C (Fig. 13) and on a powder heated in 15 ml/min dry air up to 375°C (Fig. 14).

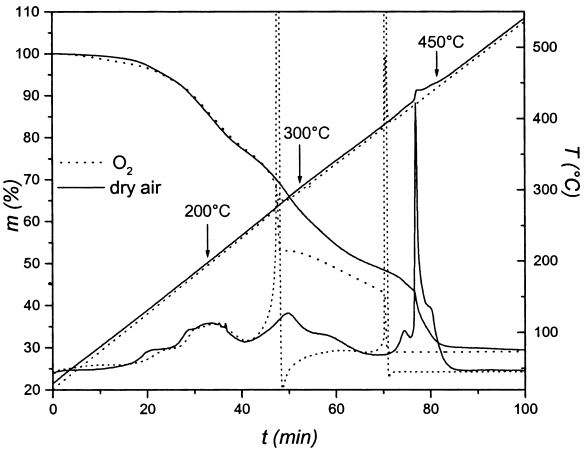

Figure 9. TGA and DTG of the BLT gel in O_2 and in dry air (5°C/min, 15 ml/min). The arrows indicate the temperatures at which the FTIR samples were taken.

The FTIR spectra (Fig. 10) show that the same decomposition intermediates are present independent of the ambient, but the decomposition occurs faster in oxygen. In oxygen the ν_{C-O} (1070 cm^{-1}) has disappeared almost completely at 300°C already. The SEM images of powders prepared at 200 and 300°C (Fig. 11) showed that the material was still very smooth: no grain structure was detected. The selected area electron diffraction (SAED, Fig. 13) TEM study of powders heated up to 310 and 350°C, showed that the resulting products are still amorphous. In Fig. 13 a bright field TEM image of the powder at 350°C is shown. It is still impossible to recognize any grain structure. However, at 375°C (Fig. 13) there are small particles (10–20 nm) present inside a smooth matrix. SAED showed that these particles are crystalline. There is only one ring of diffraction spots visible, but the d-value can be ascribed to the most intense diffraction peak (117) of the Aurivillius phase ($d = 2.97$ Å). In none of these TEM studies, however, any secondary phase was found. At 450°C all of the organic matter has clearly decomposed completely, as is seen in the FTIR spectrum (Fig. 10). There are only metal oxide bands (1000 cm^{-1}) present, next to water artefact bands (around 1600 cm^{-1} and >3500 cm^{-1}). SEM BSE (back scattered electron) images taken of the gel after heating in oxygen up to 400, 450 and 750°C (Fig. 11), show the presence of discrete particles with different chemical compositions as

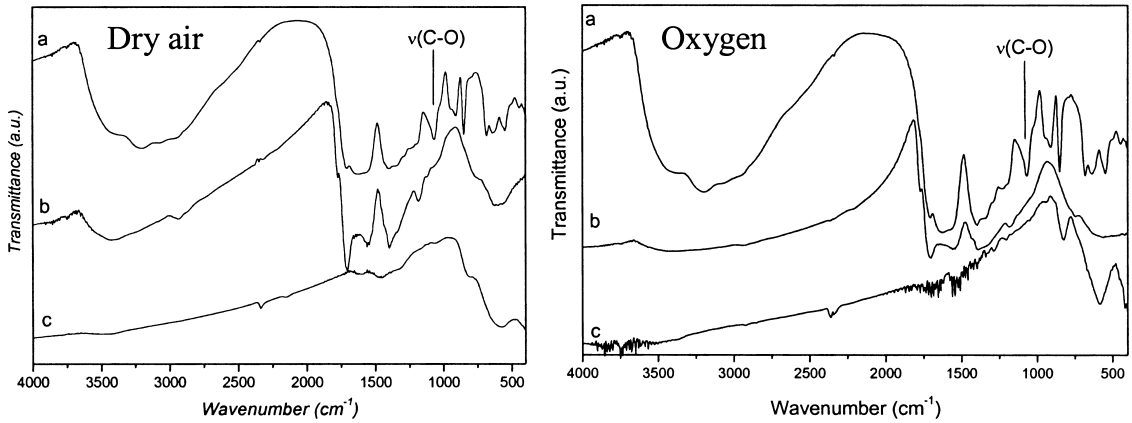

Figure 10. FTIR spectra of the BLT gel after heating at 5°C/min in 15 ml/min of dry air or O_2 to (a) 200°C, (b) 300°C and (c) 450°C.

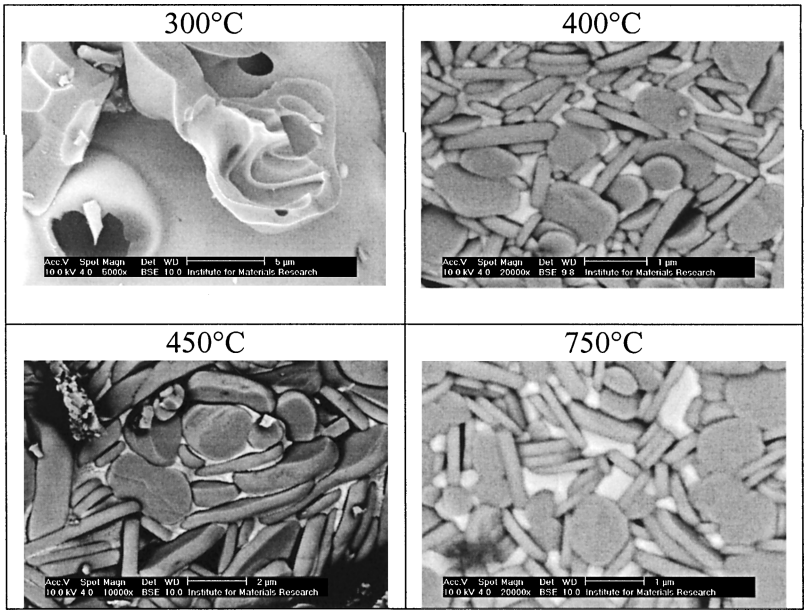

Figure 11. BSE SEM images of the BLT gel after heating in oxygen up to different temperatures, leading to a mixture of Aurivillius phase (grey) and Bi^{3+} rich Sillenite phase (white) particles.

shown in Fig. 11. Note that the gel had decomposed completely even at 400°C due to the exothermic combustion, which is impossible to stop halfway. From EDX analysis it became clear that the white areas are enriched in bismuth, as compared to the grey particles. By combination with the XRD results published earlier [11], it is concluded that the white particles have the Sillenite structure ($Bi_{12}TiO_{20}$), while the grey are Aurivillius phase ($(Bi,La)_4Ti_3O_{12}$).

In dry air the decomposition occurs slower than in oxygen. The ν_{C-O} is present as a more intense shoulder in the FTIR spectrum at 300°C in dry air than in oxygen (Fig. 10(b)). After heating up to 375°C, only amorphous material was detected with TEM (Fig. 14). At 450°C, FTIR proved that a small amount of organic matter still remains in the powder (bands between 1700 and 1150 cm^{-1}), while below 1000 cm^{-1} metal oxide bands can be distinguished. The SEM study demonstrated that the smooth morphology remains present until right before the final decomposition step (300 and 400°C, Fig. 12). However, at the end of and beyond the final decomposition step (450 and 750°C) a

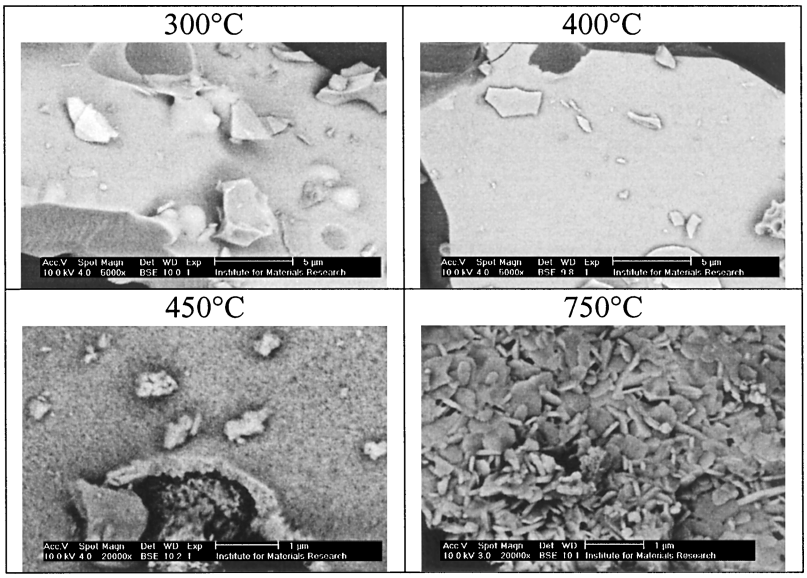

Figure 12. BSE SEM images of the phase pure BLT after heating in dry air up to different temperatures leading to phase pure BLT Aurivillius structured oxide.

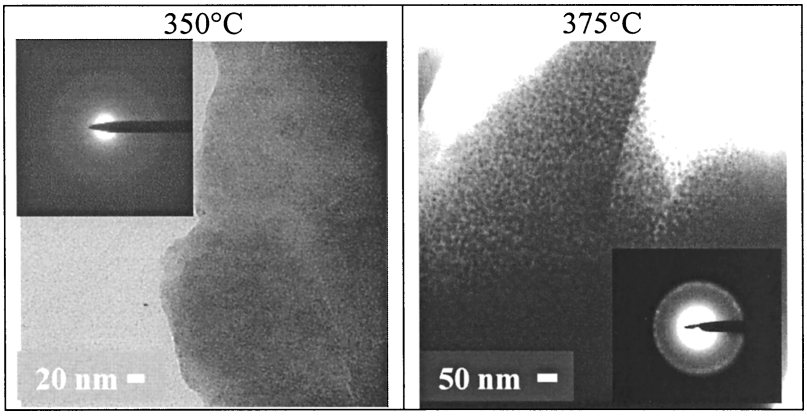

Figure 13. TEM bright field images and SAED of the BLT gel on a formvar grid after heating up to 350 and 375°C in oxygen (15 ml/min).

grain structure was seen in the SEM images (Fig. 12). There was no secondary phase detected in BSE images at any temperature after heating in dry air.

The ν_{C-O} can be used as an indicator for the coordination of the ligands to the metal ions. Its disappearance indicates the breaking of the C─O bond of citric acid's deprotonated and coordinated alcohol group and the complex is thus destabilized. For oxide crystallization to be able to start, the decomposition of the complexes is required. In oxygen the complexes are destabilized at a lower temperature, as shown by the FTIR results, which leads to a lower crystallization temperature. However, even though a monometal ion Bi^{3+}-gel is able to crystallize as metallic Bi and Bi_2O_3 at temperatures as low as 375°C and even though the metal ion complexes in the BLT gel are destabilized at 300°C already (seen from the decrease of the ν(C─O) intensity), the Bi^{3+} segregation could not be shown to occur at this temperature during decomposition of the BLT gel.

In conclusion, we have strong evidence that the segregation of the Bi^{3+} rich phase occurs during the final decomposition step (400°C), while there was already some Aurivillius phase BLT forming at 375°C.

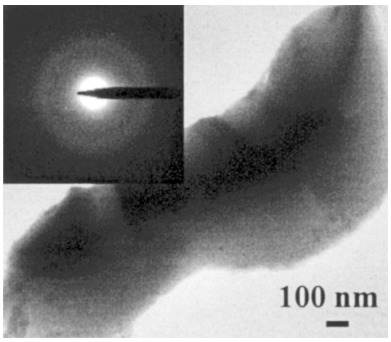

Figure 14. TEM bright field images and SAED of the BLT gel on a formvar grid after heating up to 375°C in dry air (15 ml/min).

Based on the observations explained above, it is suggested that the formation of the Sillenite phase in oxygen is due to a combination of two effects. First, in oxygen the metal ion complexes are decomposed at a lower temperature. More importantly, the stronger development of heat during the final decomposition step in oxygen compared to dry air, leads to a higher Bi^{3+} ion mobility, which possibly results in a locally higher Bi^{3+} concentration favouring the crystallization of a Bi^{3+} rich oxide.

4. Conclusion

It has been shown that the synthesis of an amorphous, nanoscale-homogeneous precursor gel is not sufficient in order to obtain a phase pure multimetal oxide after thermal decomposition. A profound understanding of the precursor gel's chemical structure, the mechanisms of thermo-oxidative decomposition reactions and oxide crystallization as a function of ambient has been achieved by integrating the results from a large amount of characterization techniques, such as FTIR and –Raman spectroscopy, thermal analysis coupled on-line to MS or FTIR, HT-DRIFT, X-ray diffraction and scanning or transmission electron microscopy. Starting from these results, an explanation for the important effect of external factors such as oxygen partial pressure on the precursor gel's thermo-oxidative decomposition pathway and phase formation mechanism has been suggested.

Acknowledgments

A. Hardy is a research assistant and G. Vanhoyland as well as M.K. Van Bael are post-doctoral research fellows of the Fund for Scientific Research – Flanders, Belgium (FWO-Vlaanderen). E. Geuzens is indebted to "het Vlaamse gewest-IWT".

References

1. B. Aurivillius, Arkiv för Kemi **1**, 499 (1949).
2. S.E. Cummins and L.E. Cross, Applied Phys. Lett. **10**, 14 (1967).
3. B.H. Park, B.S. Kang, S.D. Bu, T.W. Noh, J. Lee, and W. Jo, Nature **401**, 682 (1999).
4. A. Hardy, K. Van Werde, G. Vanhoyland, M.K. Van Bael, J. Mullens, and L.C. Van Poucke, Thermochimica Acta **397**, 143 (2003).
5. A. Hardy, D. Mondelaers, G. Vanhoyland, M.K. Van Bael, J. Mullens, and L.C. Van Poucke, J. Sol–Gel Sci. Techn. **26**, 1103 (2003).
6. A. Hardy, D. Mondelaers, M.K. Van Bael, J. Mullens, L.C. Van Poucke, G. Vanhoyland, and J. D'haen, J. Europ. Ceram. Soc. **24**, 905 (2004).
7. D. Nelis, K. Van Werde, D. Mondelaers, G. Vanhoyland, H. Van Den Rul, M.K. Van Bael, J. Mullens, and L.C. Van Poucke, J. Sol–Gel Sci. Tech. **26**, 1125 (2003).
8. K. Van Werde, D. Mondelaers, G. Vanhoyland, D. Nelis, M.K. Van Bael, J. Mullens, L.C. Van Poucke, B. Van Der Veken, and H.O. Desseyn, J. Mater. Sci. **37**, 81 (2002).
9. D. Nelis, K. Van Werde, D. Mondelaers, G. Vanhoyland, M.K. Van Bael, J. Mullens, and L.C. Van Poucke, J. Europ. Ceram. Soc. **21**, 2047 (2001).
10. K. Van Werde, G. Vanhoyland, D. Nelis, D. Mondelaers, M.K. Van Bael, J. Mullens, and L.C. Van Poucke, J. Mater. Chem. **11**, 1192 (2001).
11. A. Hardy, G. Vanhoyland, M.K. Van Bael, J. Mullens, and L.C. Van Poucke, J. Europ. Ceram. Soc. **24** (9) 2575 (2004).
12. J. Mullens in *Handbook of Thermal Analysis and Calorimetry*, edited by P.K. Gallagher; Vol. 1. *Principles and Practice* Chapter 12, EGA—Evolved Gas Analysis, edited by M.E. Brown (Elsevier, 1998), p. 509.
13. K. Nakamoto, *Infrared and Raman Spectra of Inorganic and Coordination Compounds Part B: Applications in Coordination, Organometallic, and Bioinorganic Chemistry* (John Wiley & Sons Inc., New York, 1997).
14. Y. Narendar, Regulating Oxide Crystallization from Pb, Mg, Nb-Carboxylate Gels, Thesis in Materials Science and Engineering, Pennsylvania State University, 1996.
15. M. Kakihana, M. Tada, M. Shiro, V. Petrykin, M. Osada, and Y. Nakamura, Inorganic Chemistry **40**, 891 (2001).
16. W.P. Griffith, J. Chem. Soc. 5248 (1964).
17. K. Nakamoto, *Infrared and Raman Spectra of Inorganic and Coordination Compounds Part B: Applications in Coordination, Organometallic, and Bioinorganic Chemistry* (John Wiley & Sons Inc., New York, 1997), p. 157.
18. V.T. Yilmaz, O. Andac, A. Karadag, and W.T.A. Harrison, J. Mol. Struct. **641**, 119 (2002).
19. R. Bonnaire, C.R. Acad. Sc. Paris série B **266**, 1415 (1968).
20. E. Casassas, L.O.L. Gustems, and R. Tauler, J. Chem. Soc., Dalton Trans. 569 (1989).
21. D.G. Brannon, R.H. Morrison, J.L. Hall, G.L. Humphrey, and D.N. Zimmerman, J. Inorg. Nucl. Chem. **33**, 981 (1971).
22. J. Fischer, L.H. Merwin, and R.A. Nissan, Appl. Spectr. **49**, 120 (1995).

23. J.N. Leichtnam, D. Schwartz, and R. Gadiou, J. Anal. Appl. Pyrol. **55**, 255 (2000).
24. R.P. Turcotte, J.O. Sawyer, and L. Eyring, Inorg. Chem. **8**, 238 (1969).
25. J.W. Medernach and R.L. Snyder, J. Amer. Ceram. Soc. **61**, 494 (1978).
26. D. Risold, B.G. Hallstedt, L.J. Gauckler, H.L. Lukas, and S.G. Fries, J. Phase Equil. 16, 223 (1995).
27. JCPDS; Powder diffraction file of inorganic phases, Joint Committee on Powder Diffraction Standards, Swarthmore. 1997.
28. Y. Narendar and G.L. Messing, Catal. Today **35**, 247 (1997).